Multilayer encapsulation using Atomic Layer Deposition and a moisture- stable silica containing nanocomposite polymer: correlation between gas permeation measurement on plastic film and performances obtained on top-emitting Organic Light-Emitting Diodes

Marion Provost (provost.marion@protonmail.com)
Université Grenoble-Alpes, CEA-LETI
Tony Maindron
Université Grenoble-Alpes, CEA-LETI
Stephane Cros
Université Grenoble-Alpes, CEA-LITEN

Article

Keywords:

Posted Date: June 15th, 2022

DOI: https://doi.org/10.21203/rs.3.rs-1734871/v1

Abstract

Thin Film Encapsulation (TFE) using a multilayer stack of inorganic and organic films is now a well-known encapsulation technology for organic electronics such as Organic Light-Emitting Diodes (OLED). It shows excellent gas barrier properties with very low WVTR, and good compatibility with flexible and transparent substrates. In this study, low-temperature Atomic Layer Deposition (ALD) serves for the fabrication of high performance Al_2O_3 inorganic barrier layers. A silica nanocomposite polymer serves as a moisture-stable interface layer in a very high barrier quality architecture of the kind [Al_2O_3 (25 nm)/nano-CP (1 µm)/Al_2O_3 (25 nm)/nano-CP (5 µm)]. The helium and water vapor quantitative gas permeation properties (HeTR and WVTR) of different intermediate TFE architectures deposited on plastic substrate (PET) are analyzed using a permeameter. These results are compared to an accelerated weathering test standard, for monolithic TFE deposited in-situ on top-emitting OLED circuits. On PET, the best TFE stack decreases the steady state permeation rate by a factor 1180 and 1650 respectively for helium and water vapor. Onto a top-emitting OLED, the long-term black spot occurrence rate drastically decreased from 100 $\%.h^{-1}$ to 3.210^{-3} $\%.h^{-1}$, attesting the successful implementation of this TFE architecture from ex-situ on PET substrate to in-situ on OLED circuits.

Introduction

In the recent years, the Thin-Film Encapsulation (TFE) technique has been widely used for the protection of most organic electronic devices such as Organic Photovoltaics (OPV), Organic Thin-Film Transistor (OTFT) and Organic Light-Emitting Diodes (OLED) which recommend the highest prerequisite of Water Vapor Transmission Rate (WVTR) down to 10^{-6} $g.m^{-2}.day^{-1}$ [1]. Gas barrier properties of TFE architectures mainly rely on the quality of thin-film inorganic layer, such as oxides, nitrides or oxinitrides, vacuum deposited by PVD, PECVD or ALD [2, 3]. The barrier efficiency is limited by the size and number of defects that arise from the deposition method itself, residual particle contamination in clean room environments, substrate flaws or structural imperfections due to an excessive coating thickness [4]. Therefore, polymer-based interface organic layers have been commonly used in between two inorganic layers, as [inorganic (n)/organic/inorganic (n + 1)], to encapsulate defects and flatten the surface of the inorganic layer (n) before the deposition of the inorganic barrier layer (n + 1). Such polymer materials also behave like a mechanical buffer layer and reduce the overall stress strain of the structure. The efficiency of the TFE technology relies on the synergy between inorganic barriers and polymeric interface layers [5]. In the end, for inorganic coatings with a high density of intrinsic defects, as those deposited by PVD, increasing the number of dyads [inorganic/organic] lengthen the diffusion pathway of water and oxygen molecules in the TFE structure, allowing reaching the very high gas barrier properties, the targeted WVTR of 10^{-6} $g.m^{-2}.day^{-1}$.

The ALD case is somehow different from the PVD one, as soon as high quality gas barrier coatings are of concern [6]. ALD allows the creation of highly conformable thin films and drastically reduces the number of intrinsic defects in the layer compared to other conventional techniques [7]. The material of choice in

ALD technology is alumina, mostly made by thermal ALD from trimethylaluminum (TMA) and H_2O precursors. The deposition temperature covers the range from room temperature to ~ 300°C and is therefore fully compatible with the organic electronic system requirements (< 100°C). Various TFE based on alumina layers made by ALD have been used on OLED devices [8–10] and displayed very low WVTR. However, the scientific community acknowledges that low temperature, ALD-deposited, alumina layers are highly sensitive to moisture and quickly degrade when they are exposed to a humid environment [11]. This is because low temperature ALD of alumina leads to films showing high residual hydrogen and carbon contents, issued from metal organic precursors and water, leading to defect-free but hygroscopic alumina film compositions that should be schematized as α-Al_xO_y:C:H rather than inorganic alumina, or strictly speaking Al_2O_3. It is therefore mandatory to protect the alumina barrier coating from moisture condensation to maintain its very high gas barrier properties during the commercial life of the component. A couple of publications have reported the need for an additional protection of alumina barrier coatings to ensure a long-lasting barrier property against moisture [12–14]. Our team reported the use of PVD-deposited SiO_X for the passivation of alumina ALD barrier films in AlQ_3-test, where SiO_X can be $x < 1$ or $x \sim 2$ [8]. The occurrence rate of black spots into the emissive area was reduced by 6 by adding the layer (25 nm) compared to a single alumina layer that degrades very fast under accelerated aging conditions. An estimated WVTR of $1{,}6x10^{-6}$ g/m²/day for the Al_2O_3 (25 nm)/SiO_x (25 nm) TFE has been provided in this work and today a couple of solutions can provide this very high barrier quality standards, using different interface layers [6]. Among them, thick organic-inorganic nano-Composites (nano-CP) offer a versatile solution in terms of processability, toughness and flexibility. Most of these systems are based on inorganic silica domains condensed by sol-gel chemistry and dispersed into an organic binder matrix [15]. A wide range of mechanical properties can be obtained by controlling the structure and phase dispersion or the organic and inorganic phases [16–19]. Fillers are usually blended to promote the mechanical strength of the polymeric matrix [20, 21]. The mass transfer properties of organic-inorganic nano-CPs are also well discussed in the literature and have been compiled by Wolf et al. [22]. The main expected effect is the increase of the permeation pathway (the tortuosity effect) which is obtained by incorporating dense fillers in the polymer matrix. Additionally, the processability of a nano-CP is also another point of interest for industrial uses. Highly cross-linked, transparent, scratch-resistant layers based on nano-CP materials can be achieved by using deposition methods such as roll-to-roll, spin or spray-coating, or even slot-die coating. Besides, by using a suitable UV-sensitive polymer matrix, UV-induced photo-polymerization of nano-CPs can be realized. This allows to harden and to pattern the nano-CP film, using one photolithography step, over dedicated active areas on the substrate. This decreases the number of temperature steps for curing, that otherwise may lead to degradation of the underlying circuit, if it is for instance an OLED or a related circuit based on fragile organic semiconductors.

The organic-inorganic nano-CP material made by a sol-gel process was previously developed to provide good mechanical performances in terms of wear resistance while being photo-patternable, and was previously described as a protection layer on top of OLED devices used in microdisplays [23, 24]. In this work, we explore the viability of the nano-CP material in a multilayer TFE as [Al_2O_3 (25 nm)/nano-CP (1

μm)/Al_2O_3 (25 nm)/nano-CP (5 μm)], where Al_2O_3 is deposited by low temperature ALD. The role of the nano-CP is twofold. First, it will passivate the underlying alumina barrier film, providing a high quality TFE with highly stable properties against moisture. Second, it will provide a smooth surface for the growth of the second alumina barrier layer film, allowing building a new gas barrier dyad to improve further the encapsulation of the thin-film encapsulated OLED. To fully characterize the TFE and to understand the synergy between the alumina and the nano-CP film, we performed different tests on the TFE. First, we used He as a preliminary inert gas for barrier measurements in order to understand basic properties of different gas barrier architectures, from a single layer to multilayer systems deposited onto plastic films. Doing so, we will be able to estimate the Helium Transmission Rate (HeTR) of the different TFE deposited on plastic substrates. In a second time, we measured the WVTR of these different TFE, deposited onto plastic substrates against H_2O vapor. This will also provide some understandings of the chemical reactivity of the TFE with moisture. In the end, we compared results obtained on gas barrier measurements to those obtained on top-emitting OLED encapsulated monolithically with the same TFE architectures. We noticed a remarkable improvement of barrier properties and moisture stability for the full TFE architecture [Al_2O_3 (25 nm)/nano-CP (1 μm)/Al_2O_3 (25 nm)/nano-CP (5 μm)].

Results

In this work, six TFE architectures have been studied, described as “S” for the single Al_2O_3 layer, “B” for the bilayer, “T” for the trilayer, and “M” for the multilayer, Table 1. The iteration from single to multilayer architectures has been chosen to understand the degradation of each material, Al_2O_3 and nano-CP, when it is exposed to moisture. In this study, three Al_2O_3 film grades are considered as “S” layers. Tree test methods for the gas barrier properties of different TFE have been performed and compared: the in-situ cumulative method based on the accelerated weathering test of the monolithic thin-film encapsulated OLED (90%HR, 60°C), and helium (HeTR) or water vapor (WVTR) gas transmission measurement through the TFE stacks deposited on 50 μm thick Polyethylene Terephthalate (PET) substrate. Schematic representations of the complete TFE stack are displayed in Supplementary Fig. S1. Al_2O_3 by ALD grown on PET, on nano-CP and on the SiO_X capping layer of OLED architecture are respectively referred as $S_{[PET]}$, $S_{[CP]}$ and $S_{[SiOx]}$.

Table 1
Details of TFE architectures studied in this work.

Description	Tag	TFE architecture			
		Inorganic Barrier 1 ($S_{[PET]}$ and $S_{[SiOx]}$)	Hybrid layer 1	Inorganic Barrier 2 ($S_{[CP]}$)	Hybrid layer 2
Single layer	S	Al_2O_3 [25 nm]			
Bilayer	B	Al_2O_3 [25 nm]	nano-CP [5 µm]		
Trilayer	T	Al_2O_3 [25 nm]	nano-CP [1 µm]	Al_2O_3 [25 nm]	
Multilayer	M	Al_2O_3 [25 nm]	nano-CP [1 µm]	Al_2O_3 [25 nm]	nano-CP [5 µm]

All He permeation measurements of different TFE on plastic substrates have been realized using a QHV-4 permeameter from Vinci Technologies. The WVTR measurements were measured with a permeameter using similar mass spectrometry technology than QHV-4 instruments [25, 26]. The quantitative gas permeation using the QHV-4 permeameter method allows to measure the permeant flux and the lag time of He and water molecules (also called time-lag, noted hereafter T_L) across the TFE [27]. The He atom diffuses easily into polymer layers and across defects in inorganic barrier layers. Hence, the steady state of the He permeation is reached after few seconds, making this method worthwhile to screen barrier properties of a large number of TFE stacks. However, as an inert gas, He does not interact with the constitutive materials of the TFE, contrary to polar water molecules. A comprehensive study of the TFE degradation under moisture diffusion is therefore mandatory. Depending on the moisture sensitivity of materials in the TFE, the TFE properties in the steady state water permeation regime can change over time. The HeTR of all samples, monitored before and after the water permeation measurement, remained constant regardless of the chemical nature (nano-CP or Al_2O_3) or the last layer in contact with water vapor (in the experiment, the TFE side is exposed to water flux). The TFE appears undamaged over the time scale of the measurement, the extrapolated WVTR therefore corresponds to the steady-state flux undisturbed by the extrinsic degradations occurring on the encapsulation (Supplementary Method). However, for a prolonged experiment, long-term degradations are likely to be observed along a rise of the WVTR values. In this case, the degradation rates will depend on the specific sensitivity against moisture of nano-CP and Al_2O_3 surfaces. The main issue with WVTR measurements, especially for very high quality TFE, is their duration, at least several days in best cases. Hence, this method cannot be used to screen different TFE cannot provide statistics and rapid quality control. As the deposition of a given TFE architecture onto a plastic film may differ from its deposition onto an OLED component, the final true test of the reliability of the TFE, for a given component to be encapsulated, must be done in the end onto the real component itself.

The accelerated weathering test on OLED devices are studied according to the methods applied for optical calcium tests [8]. Results are expressed as the percentage of defective OLED as a function of the storage time. First a significant number of defects appears on the surfaces with a high occurrence rate due to pinholes in the barriers. Secondly, at intermediate time, the steady regime is obtained showing a lower defect occurrence rate while existing defects grow and propagate. Finally, at a longer time span the barrier may start to degrade leading to a final increase of the defect rate.

Table 2
Time-lag and calculated BIF from helium and water vapor measurement of the studied TFE on PET substrate and from in-situ OLED weathering tests (Raw data displayed in Supplementary S2-S5).

TFE Tag	HeTR data			WVTR data			In-situ OLED weathering test		
	T_L (s)	BIF_{PET}	$BIF_{PET/S}$	T_L (h)	BIF_{PET}	$BIF_{PET/S}$	T_L (h)	$BIF_{OLED/S}$ α_1	$BIF_{OLED/S}$ α_2
S	Instant	37 ± 7	1	21 ± 13	259 ± 38	1	92.0	1	1
B	8.5 ± 0.6	226 ± 45	6 ± 2	23 ± 7	581 ± 58	2.3 ± 0.3	99.7	7.5	1.3
T	9.9 ± 0.3	392 ± 62	10 ± 3	43.1	757	3.0 ± 0.4	109.7	13.8	10.9
M	11.1 ± 3	1178 ± 252	29 ± 11	27	1646	6.4 ± 0.5	113.3	17.5	13.8

The gas barrier efficiency of the different TFE architectures has been expressed as the Barrier Improvement Factor (BIF) regarding a given substrate architecture and compared in Table 2 [25, 26, 28]. BIF_{PET} expresses the improvement factor of the TFE deposited on the PET substrate. Such improvement cannot be calculated on raw OLED as they are quickly destroyed during the test. As a result, $BIF_{PET/S}$ and $BIF_{OLED/S}$ express the improvement factor of the additional layers of the TFE, processed on the first inorganic layer S, respectively for PET substrates and OLED circuits. The BIF has been calculated as the ratio between the steady-state gas flux of the given substrate (PET, PET/S, etc.) and the steady-state flux of the complete substrate/TFE stack. A BIF exceeding unity represents therefore an improvement of the gas barrier properties of the substrate/TFE compared to the single substrate. A BIF below unity is the consequence of a substrate degradation.

Discussion

The different TFE were first individually studied on PET substrates. As expected, going from single to multilayer architectures decreases the steady state flux and significantly increases the BIF for both helium and water vapor measurements. The T_L also increases accordingly (Table 2). Best results were obtained for M, which improved the gas barrier properties of the PET substrate by a factor 1178 and 1646, respectively for helium and water vapor permeation.

A linear correlation can be found by plotting the helium BIF as a function of water vapor BIF on PET substrates (Fig. 1). According to the experimental results, the linear slope of the fit is 0.42 ± 0.08. HeTR of the TFE were measured before and after the WVTR experiment and remained constant. It was concluded that the stack does not suffer any moisture ingress over the duration of the WVTR measurement. Then, the correlation between Helium and water vapor BIF can be used as a predictive scale for quality screening of the TFE and control samples can regularly be added to the fabrication of the TFE and characterized to anticipate shifts of performances due to process variations (aging of the reagent, particle contamination, etc.). The chemical selectivity of the substrate between helium and water depends on the materials used for the TFE. New studies should be considered for any change in the chemical composition.

As previously stated, in the TFE architecture the barrier properties are mainly provided by the Al_2O_3 barrier layer, and high performances are not expected from the nano-CP material. Indeed, as shown in (Table 2) the TFE S displays an average BIF of 37 while the BIF provided by a single nano-CP layers barely exceed unity (Supplementary Table S6). M and B architecture are respectively compared with T and S to highlight the influence of the thick nano-CP layer. Despite displaying no intrinsic barrier properties, the 5 µm thick nano-CP coating improved by a factor 2.3 the performances of architecture S and T regarding the water vapor steady state flux, and positively impacted the T_L. Firstly, this evolution obviously implies that the processing of this material (solvent, temperature, polymer shrinkage, etc.) has at least no negative impact on the quality of the barrier layer underneath, which is consistent with our previous observations on OLED substrates [23, 24]. To go into detail, as previously observed in the literature over different conditions, the protective effect cannot be explained by the poor intrinsic properties of the polymer-based materials and is closely linked to the barrier layer substrate [8, 29, 30]. Some studies suggest that the hydrophobic properties of the resin may explain the passivation differences as the coating isolates the barriers from the sorption of ambient moisture [31]. Yet, a global consensus is to be found regarding this hypothesis. In this study, this assumption is consistent with our materials but may not be sufficient to explain the overall decrease in steady-state flux as the samples are stored under inert atmosphere prior to the measurement. Another hypothesis relies on the mechanical properties; the TFE is deposited on flexible substrate and inevitably mechanically stressed over the test. The top coating is expected to prevent degradations originating from the storage and the handling of the substrate such as bending stress, surface scratches from the permeation equipment and particle deposition. As a result, the BIF, the reproducibility as well as the time-lag are slightly improved for mechanically protected samples.

Table 3
Helium and water vapor gas barrier improvement relatively to the substrate material.

Al_2O_3 grade	Substrate	BIF of layer S [Al_2O_3]			BIF of dyad [Al_2O_3/nano-CP]		
		TFE	HeTR	WVTR	TFE	HeTR	WVTR
$S_{[PET]}$	PET	S	37 ± 7	259 ± 38	B	226 ± 45	581 ± 58
$S_{[CP]}$	B	T	1.6 ± 0.4	1.3 ± 0.3	M	5.0 ± 1.3	2.9 ± 0.7

In the TFE architecture, the nano-CP is not only considered as covering material but also as an interface planarization layer. It is well known that the ALD method is sensitive to the properties of the substrates [32–34] (roughness, surface energy); therefore the analysis of the impact on our Al_2O_3 growth and on the overall barrier performances is required ($S_{[PET]}$, $S_{[CP]}$ and $S_{[SiOx]}$). A WVTR of 3.1 10^{-2} g.m^{-2}.day^{-1} is measured from the single layer $S_{[PET]}$ (Supplementary Fig. S3). This result is abnormally high compared to the average data detailed in the literature [7, 35] (10^{-3} to 10^{-5} g.m^{-2}.day^{-1}), and is attributed to a deteriorated growth of the Al_2O_3 by ALD on top of the polymeric PET substrate. This result was to be expected and is corroborated by a previous observation of the same ALD growth made at CEA-LETI [36]. On top of a commercial organic photoresist the Al_2O_3 layers are imperfect and granular, while layers grown on low-roughness silicon substrate are smooth and homogeneous. In the Table 3, the quality of the two Al_2O_3 grade $S_{[PET]}$ and $S[_{CP]}$ respectively grown on PET and nano-CP surface are compared for both the single layer S and the very same layer S included in the dyad Al_2O_3/nano-CP. The $S_{[CP]}$ quality grade displays lower performances than the grade $S_{[PET]}$. BIF are respectively decreased by a factor 30 and a factor 200 for HeTR and WVTR measurement. The nano-CP is known to be smooth (0.75 ± 0.15 nm, RMS 500*500 nm scan), yet the presence of asperities due to embedded particle contamination can explain the BIF gap with a layer grown on PET ($S_{[PET]}$). Another possibility concerns the surface porosity; in the case of the presence of dead volumes in the surface of the composite, the $S_{[CP]}$ layer may grow in these defects and lose quality. Finally, the surface energy of the material can also interfere with the sorption of the ALD reagent and the growth mechanisms. Nevertheless, even if the morphology of the $S_{[CP]}$ layer is affected, the addition of new layers and dyads significantly increase the barrier performances of the TFE. The morphology of Al_2O_3 layers obtained by ALD layer is more homogeneous on top of smooth inorganic substrates. The measurements using PET substrate are likely to underestimate the real in-situ permeation rate on top of the SiO_X capping layer during the fabrication of the OLED substrate ($S_{[SiO]}$). In our laboratory, OLED devices encapsulated with the single $S_{[SiOx]}$ barrier can be stored over months in ambient conditions without displaying any degradation. Al_2O_3 quality grades are expected to improve as follows: $S_{[CP]} < S_{[PET]} < S_{[SiOx]}$.

These observations highlight the fact that the intrinsic performances and synergistic influence of each layer need to be evaluated to study the performances of the complete TFE and to anticipate the additions of new layers to further enhance the barrier properties. For this and other reasons, gas permeation

measurement are not easily transferred to other methods such as in-situ weathering as long as the substrate impact the studied materials.

The OLED device itself is the most sensitive indicator of the performance of the TFE. Previous experiments have been performed in our laboratory using dedicated fluorescent molecular films encapsulated with the Al_2O_3 barrier layers, defects have been observed as non-emitting singularities under UV light excitation [37]. Working on a full device is expensive and time-consuming, but it allows an extended approach as nearly all the constitutive layers in the OLED architecture are sensitive against moisture and oxygen [38]. Black spots appear due to the morphological evolution of the organic semiconductors, but mainly because of the degradation of the metallic electrodes and the loss of electrical contact (Fig. 2). Each additional layer can influence the development of extrinsic degradation and the lifetime of the device, it makes the final performances difficult to predict and to standardize. In order to study the in-situ performances of the TFE standard accelerated weathering tests in damp and hot storage environment need to be considered.

Putting aside the variation of ALD growth mechanisms, in-situ weathering test and WVTR measurement are uneasy to compare due to two main differences. First, WVTR measurement on flexible PET substrate are more affected by the mechanical ingress (bending stress, scratches from manipulation), but in-situ measurement affects the TFE as well as the OLED component (changes in internal stress leading to delamination of the TFE). Secondly, the experimental conditions differ. WVTR measurement is based on 38°C-100%HR climatic condition and proceed by applying a controlled pressure and ultra-high vacuum around the membrane. In-situ measurement consists of a storage under 60°C-90%HR climatic conditions. Water diffusion through the TFE is driven by the temperature and water partial pressure. Arrhenius extrapolation can be used as a first approximation; however, this model fails to consider the thermal and chemical changes of the membrane during in-situ measurement. During in-situ weathering tests, substrate is impacted by the method and its morphology changes over time. The constitutive layers of the OLED substrate (electrodes, capping SiO_X) influence the permeation properties as intrinsic degradations creates voids and cracks in the architecture. Moreover, like most ceramics and polymer-based materials the nano-CP is sensitive to moisture ingress. A slight irreversible increase in tensile stress (7 ± 1 MPa) can be observed after 50 days of storage (21°C, 50%HR) due to chemical reactions of the silica fillers [39]. This mechanism as well as the thermal dilatation of the layers is amplified in damp and hot environment and can lead to cracking or disbonding. However, in this study no failure of this kind was observed on the nano-CP as long as the protocol avoid brutal thermal chocs. Only black spots appeared and grew over time during the weathering test (90%HR, 60°C).

Over 500h of test, the first two regimes of degradation are observed on the samples: high defect occurrence, followed by a slower occurrence completed by the growth of existing defects (Supplementary Fig. S4). The defect occurrence rates are represented by the slope of the linear fit versus time and respectively expressed as (α_1) and (α_2). The lag-time (T_L) of this experiment express the transition between the two regimes and is determined graphically as the intersection of the linear regressions. Similarly to the HeTR and WVTR experiment, the defect occurrence rate followed the previous observation

on PET substrate and the protection was enhanced from TFE (S) < TFE (B) < TFE (T) < TFE (M) as displayed in Table 2. This observation attests the successful implementation of the process from ex-situ deposition on PET substrate to in-situ monolithic deposition on the fragile OLED component. As a reference, bare OLED circuits are destroyed within hours under 60°C-90%HR storage conditions. After 500h of storage, $S_{[SiOx]}$ and B TFE protected respectively 2.7% and 67.6% of the circuits. Best results were obtained for T and M with an average of 90.8% remaining flawless OLED surfaces. In this case, the defects mainly occurred during the initial stage of the test.

At the early stage, the first defect occurrence rate (α_1) is due to initial encapsulation defects on the TFE coming from the fabrication process and the handling of the substrates. The complete TFE architecture M improved the performances of the initial $S_{[SiOx]}$ layer by a factor 17.5. On OLED circuits the TFE are not mechanically stressed, yet the nano-CP also surprisingly displayed a positive influence on the occurrence rate. BIFα_1 due to nano-CP layer alone are respectively 7.5 and 1.3 for B and M architecture (Supplementary Table S6). This result still cannot be explained by the intrinsic gas barrier properties of the nano-CP itself but can be attributed in this case to the defect encapsulation properties of the resin. Nanoparticle contamination is molded and kept in place into the layer, avoiding the formation of new pinholes [40]. Nano-CP layers indirectly influence the rate by reducing the defect occurrence of the barrier layer. As previously described on PET substrate, the addition of the second Al_2O_3 layer $S_{[CP]}$ does not give a significant rise to the T_L of the TFE and the BIFα_1 (1.8) is extremely low (Table 3). These results are consistent with the hypothesis of a degraded growth leading to poorer performances. Although the $S_{[CP]}$ barrier slightly improves the barrier properties, the main protection and the defect occurrence α_1 is mainly linked to the quality of the first barrier $S_{[SiOx]}$.

The second defect occurrence rate (α_2) is due to the steady-state degradation of the barrier and growth of existing defects. In this case, the architecture M Improved the performances of the $S_{[SiOx]}$ layer by a factor 13.8. BIFα_2 due to the nano-CP covering layer is only 1.3 in both B and M architecture which is consistent with the poor steady-state intrinsic barrier properties of the nano-CP material (Supplementary Table S6). Two ranges of defect occurrences can be observed, corresponding to one or two barrier layers in the TFE. Despite a flawed morphology, the addition barrier layer $S_{[CP]}$ significantly improved the long-term properties (BIFα_2 8.7). A small improvement of the T_L is observed, this result can be due to the lengthening of the permeation pathway. Another possibility relies on the getter effect, protecting the subjacent layer from absorbed water molecules.

The amount of defective OLED protected with the complete TFE M is causally linked to the occurrence rate α_1, that is, to the quality of the $S_{[SiOx]}$ layer and thus to the amount of particle contamination arising from the fabrication process reactors (OLE

D and ALD) as well as the nature and the flatness of the substrate. Supplementary layers show a smaller positive effect on the BIF improvement, and yet are mandatory to fully achieve the required gas barrier properties (Table 2, Table 3). Correlation between in-situ weathering test on OLED and ex-situ permeation

test on PET substrate needs to consider the chemical and morphological changes of the TFE. In this study, assuming that the WVTR measurement did not record significant degradations of the TFE due to moisture ingress, then the $BIF_{PET/S}$ can be compared to the $BIF_{OLED/S}$ α1 (Fig. 3). Both are causally linked to the defect occurrence in the inorganic layer of the TFE caused by the fabrication process (nanoparticle contamination, solvent ingress) and by the handling of the substrates (bending stress, scratches). The steady state degradation of the OLED substrate (α_2) cannot be predicted by the WVTR measurement done in the 38°C-100%HR conditions. In order to approach a correlation, new experiment could consider changing the WVTR condition, or storing the TFE on PET substrate in a climatic chamber for a given time before starting the WVTR measurement.

Conclusion

In TFE architectures, the gas barrier properties are usually provided by the inorganic barrier layers and the intrinsic performances of the polymer-based interface materials have low impact on the stack. The performance of the membrane is usually enhanced by the repetitive addition of new organic-inorganic dyad as the length of the permeation path increases. In this study, barrier properties are mainly due to a high-performance initial barrier layer which is protected by the rest of the stack. In this case, only three additional layers are enough to achieve the protection of OLED devices. The nano-CP resin used as an interface and covering layers displays good surface qualities (low roughness, hydrophobicity) and enhanced mechanical properties (bending, wear resistance). The contribution of the nano-CP resin to the global gas barrier mechanism mainly relies on the mechanical protection of the subjacent layer and the passivation of preexisting defects. This material is also a suitable candidate for the growth of the next barrier layer. Helium permeation measurement allowed an easy and fast preliminary comparison of the TFE and comprehension of the permeation mechanisms. Moreover, a correlation between helium and water vapor permeation can be built, providing an easy quality control tool for the fabrication processes. As defects can also arise from the OLED fabrication itself, and harsher environment in terms of temperature and moisture, in-situ weathering tests are mandatory to complete the study.

Methods

Top-emitting OLED and PET Substrates. Two kinds of substrates were used for this study: silicon (Si) wafers containing top-emitting OLED for in-situ weathering tests and commercial 50 µm PET substrates (Cosmoshine) for permeation measurements. The top emitting OLED have been fabricated onto 200nm-wide Si substrates, as previously described in other studies [23, 24, 41]. To avoid any influence of the OLED batch, all the TFE conditions are shared on every silicon substrate (~ 350 OLED).

Gas barrier layers. The Al_2O_3 barrier layers (25 nm) have been deposited by Atomic Layer Deposition (ALD) in a Savannah 200 Series (Cambridge Nanotech), hermetically embedded in a nitrogen filled glove box system (MBraun). The ALD process has been performed at 90°C using tri-methylaluminum (TMA)

and water (H_2O) precursors. One cycle consists of a H_2O pulse, H_2O purge, TMA pulse and TMA purge successively. Nitrogen was used as both the reagent carrier and the purge gas.

Interface and covering materials. The silica nanoparticle embedded acrylate nanocomposite resin (nano-CP) is composed of methacrylate-modified silica nanoparticles dispersed in an acrylate polymer matrix. First, tetraethyl orthosilicate (TEOS) (Dynasylan A, Evonik Co., Germany), used as silica source, was diluted in an ethanol-methanol medium and condensed by sol-gel process under basic ammonia catalysis (ABCR GmbH, Germany). This method leads to the formation of dense spherical nanoparticles around 9 nm wide. The size was monitored by Dynamic Light Scattering (DLS, Vasco Cordouan tech.) and Transmission Electron Microscopy (TEM, Jeol 3010, 300 kV, LaB6 filament). During a second step, 3-methacryloxypropyl triethoxysilane (Dynasylan MEMO, Evonik Co., Germany) was grafted onto the silica domains under the same catalytic conditions to produce the methacrylate-modified silica suspension. The molar ratio of TEOS:MEMO is 1:0.3. The mixture was then distilled to remove the excess solvent and mixed with pentaerythritol tetraacrylate monomers (Arkema, France), to obtain a final inorganic volume percentage of 35%. Bis(2,4,6-trimethylbenzoyl)-phenylphosphineoxide, (Omnirad 819, IGM Resins, France) was used as a radical photo-polymerization initiator. The acrylated reference resin ($R_{nano-CP}$) is prepared by mixing the pentaerythritol tetraacrylate monomers and the photo-polymerization initiator with appropriate solvents. This formulation corresponds to the organic host of the nano-CP material exempt from the silica fillers.

Thin-film encapsulation architecture (TFE). The TFE architectures were obtained by the successive deposition of inorganic Al_2O_3 barrier layers by the low temperature ALD. The nano-CP resin was deposited by spin-coating method and cured under UV light centered at 365 nm (MA8 Semi-automatic Mask Aligner, SUSS Microtec) after a suitable low-temperature baking step (< 100°C). Thicknesses were tuned according to the viscosity of the liquids. In order to save the electrical contact pads of the OLED, a Cr-based photomask was used to pattern the resin around the OLED active surfaces (see Supplementary Fig. S1). The excess material was removed using a suitable solvent-based developer and the development step was made onto an EVG150 tool from EVG Group. Al_2O_3 barrier layers do not need to be patterned to recover the electrical bonding [42]. The TFE are processed in-situ, in a clean-room environment and after a prior cleaning step of the substrate to avoid any particle contamination. The different samples were stored under nitrogen atmosphere in the glove-box system (MBraun) between the fabrication steps. The storage under ambient condition was kept down to a minimum over the characterization time.

Permeation test methods. Helium gas permeation measurements on PET substrate were performed using a helium permeameter constructed by Vinci Technologies (QHV-4) under a controlled temperature of 38°C and hygrometry (0%). Water vapor gas permeation measurements were performed using patented homemade permeameters under a controlled temperature of 38°C and hygrometry (100%) [25]. In both cases, the samples were positioned between an upstream chamber filled with the permeant gas at a controlled pressure and a downstream ultra-high vacuum chamber. A quadrupolar analyzer and ion trap mass spectrometer (MSK, E-vision+) was used as a detector. Regarding water vapor measurements,

isotopes (heavy water 99% $_2H_2O$ (Eurisotop)) are used as permeant and allow to distinguish the signal from the atmosphere or adsorbed contamination. The daily fluctuation of the equipment is controlled using a calibrated helium leak for helium measurements (QHV-4) and known 100 µm PET sample for water vapor measurements.

Accelerated weathering tests. The OLED substrates were stored at 60°C under 90%HR on a controlled environmental chamber (VC0020, Vötsch). At the end of a cycle, the samples slowly returned to room temperature (~ 1°C/min, ~ 3%HR/min). The presence of dark spots in the emissive area, crack or delamination was tightly controlled for each circuit before the test and after 24, 48, 250 and 500 hours using a HD camera integrated on an automatic wafer prober (Tel P8XL). To ensure the reproducibility of the test: a median number of 65 initially perfect OLED circuits were measured per TFE condition and the tested OLED were picked from at least two different silicon substrates to check on the influence of OLED fabrication. In this study, an OLED surface (0.38”) is considered damaged in the early stage of the degradation process as soon as a singular dark spot is noticeable on the emitting area. In some rare case, small dark spots without any further degradation over the time appeared, this mechanism is attributed to intrinsic defects causing shortcuts and these samples were not taken into consideration.

Declarations

Acknowledgements

This study is part of a PhD thesis under French funding from AID/DGA (Defense Innovation Agency, French Ministry of Defense). Authors would like to thank Rose-Marie Sauvage from AID/DGA for her follow-up support during the project and Polyrise SAS for their technical support.

Autor Contributions

MP managed the research activity planning and execution, developed the chemistry and architecture of the studied TFE, carried out the HeTR and weathering test experiments and analysed the data. **TM** supervised the project and provided the instrumentation analysis and fabrication tools for OLED substrates. **SC** provided the instrumentation and analysis tools for gas permeation measurement, carried out the WVTR experiments. **All authors** wrote the manuscript and collaborated on the theoretical analysis of the data.

Data availability statement

The datasets generated during and/or analyzed during the current study are available from the corresponding authors on a reasonable request.

Additional information

The funding sources have no involvement in the study design, in the collection, analysis and interpretation of data and in the writing of the report. The authors declare that they have no conflict of interest.

References

1. Yu, D., Yang, Y.-Q., Chen, Z., Tao, Y. & Liu, Y.-F. Recent progress on thin-film encapsulation technologies for organic electronic devices. Opt. Commun. **362**, 43–49 (2016).
2. Jeong, E. G., Kwon, S., Han, J. H., Im, H.-G., Bae, B.-S. & Choi, K. C. A mechanically enhanced hybrid nano-stratified barrier with a defect suppression mechanism for highly reliable flexible OLEDs. Nanoscale **9**, 6370–6379 (2017).
3. Amberg-Schwab, S. in *Handb. Sol-Gel Sci. Technol. Process. Charact. Appl.* (eds. Klein, L., Aparicio, M. & Jitianu, A.) 3295–3315 (Springer International Publishing, 2018). doi:10.1007/978-3-319-32101-1_72
4. da Silva Sobrinho, A. S., Czeremuszkin, G., Latrèche, M. & Wertheimer, M. R. Defect-permeation correlation for ultrathin transparent barrier coatings on polymers. J. Vac. Sci. Technol. A **18**, 149–157 (2000).
5. Graff, G. L., Williford, R. E. & Burrows, P. E. Mechanisms of vapor permeation through multilayer barrier films: Lag time versus equilibrium permeation. J. Appl. Phys. **96**, 1840–1849 (2004).
6. Lee, S., Han, J.-H., Lee, S.-H., Baek, G.-H. & Park, J.-S. Review of Organic/Inorganic Thin Film Encapsulation by Atomic Layer Deposition for a Flexible OLED Display. JOM **71**, 197–211 (2019).
7. Carcia, P. F., McLean, R. S., Reilly, M. H., Groner, M. D. & George, S. M. Ca test of Al2O3 gas diffusion barriers grown by atomic layer deposition on polymers. Appl. Phys. Lett. **89**, 031915 (2006).
8. Maindron, T., Jullien, T. & André, A. Defect analysis in low temperature atomic layer deposited Al2O3 and physical vapor deposited SiO barrier films and combination of both to achieve high quality moisture barriers. J. Vac. Sci. Technol. Vac. Surf. Films **34**, 031513 (2016).
9. Han, Y. C., Kim, E., Kim, W., Im, H.-G., Bae, B.-S. & Choi, K. C. A flexible moisture barrier comprised of a SiO2-embedded organic–inorganic hybrid nanocomposite and Al2O3 for thin-film encapsulation of OLEDs. Org. Electron. **14**, 1435–1440 (2013).
10. Choi, H., Shin, S., Jeon, H., Choi, Y., Kim, J., Kim, S., Chung, S. C. & Oh, K. Fast spatial atomic layer deposition of Al2O3 at low temperature (< 100°C) as a gas permeation barrier for flexible organic light-emitting diode displays. J. Vac. Sci. Technol. Vac. Surf. Films **34**, 01A121 (2015).
11. Nam, T., Lee, H., Seo, S., Cho, S. M., Shong, B., Lee, H.-B.-R. & Kim, H. Moisture barrier properties of low-temperature atomic layer deposited Al2O3 using various oxidants. Ceram. Int. **45**, 19105–19112 (2019).
12. Keuning, W., van de Weijer, P., Lifka, H., Kessels, W. M. M. & Creatore, M. Cathode encapsulation of organic light emitting diodes by atomic layer deposited Al2O3 films and Al2O3/a-SiNx:H stacks. J. Vac. Sci. Technol. A **30**, 01A131 (2012).

13. Carcia, P. F., McLean, R. S., Groner, M. D., Dameron, A. A. & George, S. M. Gas diffusion ultrabarriers on polymer substrates using Al2O3 atomic layer deposition and SiN plasma-enhanced chemical vapor deposition. J. Appl. Phys. **106**, 023533 (2009).
14. Bertrand, J. A. & George, S. M. Evaluating Al2O3 gas diffusion barriers grown directly on Ca films using atomic layer deposition techniques. J. Vac. Sci. Technol. A **31**, 01A122 (2013).
15. Mammeri, F., Bourhis, E. L., Rozes, L. & Sanchez, C. Mechanical properties of hybrid organic–inorganic materials. J. Mater. Chem. **15**, 3787–3811 (2005).
16. Shimizu, T., Kanamori, K. & Nakanishi, K. Silicone-Based Organic–Inorganic Hybrid Aerogels and Xerogels. Chem. – Eur. J. **23**, 5176–5187 (2017).
17. Balazs, A. C., Emrick, T. & Russell, T. P. Nanoparticle Polymer Composites: Where Two Small Worlds Meet. Science **314**, 1107–1110 (2006).
18. Scully, A. D., Mao, Q. & Fell, C. J. High-performance oxygen barrier inorganic–organic coating for polymeric substrates. Surf. Coat. Technol. **239**, 222–226 (2014).
19. Provost, M., Raulin, K., Maindron, T. & Gaud, V. Influence of silane coupling agent on the properties of UV curable SiO2-PMMA hybrid nanocomposite. J. Sol-Gel Sci. Technol. **89**, 796–806 (2019).
20. Amerio, E., Fabbri, P., Malucelli, G., Messori, M., Sangermano, M. & Taurino, R. Scratch resistance of nano-silica reinforced acrylic coatings. Prog. Org. Coat. **62**, 129–133 (2008).
21. Malzbender, J., de With, G. & den Toonder, J. M. J. Elastic modulus, indentation pressure and fracture toughness of hybrid coatings on glass. Thin Solid Films **366**, 139–149 (2000).
22. Wolf, C., Angellier-Coussy, H., Gontard, N., Doghieri, F. & Guillard, V. How the shape of fillers affects the barrier properties of polymer/non-porous particles nanocomposites: A review. J. Membr. Sci. **556**, 393–418 (2018).
23. Provost, M., Suhm, A., Gaud, V., Raulin, K., Mandrillon, V. & Maindron, T. 75 – 3: UV-curable Thin-film Packaging for OLED-based Microdisplays. *SID Symp. Dig. Tech. Pap.* **49**, 1007–1010 (2018).
24. Maindron, T., Chambion, B., Provost, M., Vandeneynde, A., Peray, P., Zussy, M., Dechamp, J., Rossat, C. & Gonnin, S. Curved OLED microdisplays. J. Soc. Inf. Disp. **27**, 723–733 (2019).
25. Morlier, A., Cros, S., Garandet, J.-P. & Alberola, N. Structural properties of ultraviolet cured polysilazane gas barrier layers on polymer substrates. Thin Solid Films **550**, 85–89 (2014).
26. Firon, M., Cros, S. & Trouslard, P. Method and device for measurement of permeation. U.S. Patent US2007186622. (2007).
27. Nisato, G., Klumbies, H., Fahlteich, J., Müller-Meskamp, L., van de Weijer, P., Bouten, P., Boeffel, C., Leunberger, D., Graehlert, W., Edge, S., Cros, S., Brewer, P., Kucukpinar, E., de Girolamo, J. & Srinivasan, P. Experimental comparison of high-performance water vapor permeation measurement methods. Org. Electron. **15**, 3746–3755 (2014).
28. Chatham, H. Oxygen diffusion barrier properties of transparent oxide coatings on polymeric substrates. Surf. Coat. Technol. **78**, 1–9 (1996).

29. Rückerl, A., Zeisel, R., Mandl, M., Costina, I., Schroeder, T. & Zoellner, M. H. Characterization and prevention of humidity related degradation of atomic layer deposited Al2O3. J. Appl. Phys. **121**, 025306 (2017).
30. Kim, H., Ra, H. N., Kim, M., Kim, H. G. & Kim, S. S. Enhancement of barrier properties by wet coating of epoxy-ZrP nanocomposites on various inorganic layers. Prog. Org. Coat. **108**, 25–29 (2017).
31. Wang, L., Ruan, C., Li, M., Zou, J., Tao, H., Peng, J. & Xu, M. Enhanced moisture barrier performance for ALD-encapsulated OLEDs by introducing an organic protective layer. J. Mater. Chem. C **5**, 4017–4024 (2017).
32. Parsons, G. N. & Clark, R. D. Area-Selective Deposition: Fundamentals, Applications, and Future Outlook. Chem. Mater. **32**, 4920–4953 (2020).
33. Ding, J. N., Wang, X. F., Yuan, N. Y., Li, C. L., Zhu, Y. Y. & Kan, B. The influence of substrate on the adhesion behaviors of atomic layer deposited aluminum oxide films. Surf. Coat. Technol. **205**, 2846–2851 (2011).
34. Parsons, G. N., George, S. M. & Knez, M. Progress and future directions for atomic layer deposition and ALD-based chemistry. MRS Bull. **36**, 865–871 (2011).
35. Jeong, E. G., Han, Y. C., Im, H.-G., Bae, B.-S. & Choi, K. C. Highly reliable hybrid nano-stratified moisture barrier for encapsulating flexible OLEDs. Org. Electron. **33**, 150–155 (2016).
36. Simon, J.-Y., Maindron, T., Aventurier, B., Gatta, S. M. D., Viasnoff, E., Jullien, T., Ghazouani, A. & Lafond, D. P.141L: Late-News Poster: ALD-based Multilayer Encapsulation of PIN OLED: On the Stability of the Organic Layer in 85°C / 85% RH Storage Conditions. *SID Symp. Dig. Tech. Pap.* **44**, 1470–1472 (2013).
37. Maindron, T., Aventurier, B., Ghazouani, A., Jullien, T., Rochat, N., Simon, J.-Y. & Viasnoff, E. Investigation of Al2O3 barrier film properties made by atomic layer deposition onto fluorescent tris-(8-hydroxyquinoline) aluminium molecular films. Thin Solid Films **548**, 517–525 (2013).
38. Azrain, M. M., Mansor, M. R., Fadzullah, S. H. S. M., Omar, G., Sivakumar, D., Lim, L. M. & Nordin, M. N. A. Analysis of mechanisms responsible for the formation of dark spots in organic light emitting diodes (OLEDs): A review. Synth. Met. **235**, 160–175 (2018).
39. Kook, S.-Y. & Dauskardt, R. H. Moisture-assisted subcritical debonding of a polymer/metal interface. J. Appl. Phys. **91**, 1293–1303 (2002).
40. In *Handb. Depos. Technol. Films Coat. Third Ed.* (ed. Martin, P. M.) 93–134 (William Andrew Publishing, 2010). doi:10.1016/B978-0-8155-2031-3.00003-X
41. Bouzid, K., Maindron, T. & Kanaan, H. Thin-film encapsulated white organic light top-emitting diodes using a WO3/Ag/WO3 cathode to enhance light out-coupling. J. Soc. Inf. Disp. **24**, 563–568 (2016).
42. Maindron, T., Troc, N., Aventurier, B., Mandrillon, V., Delaye, V. & Vandeneynde, A. P-183: Study of Electrical Probing through Thin-film Encapsulation Made of Al2O3 Films Deposited by Low Temperature ALD onto Different Metallic Underlayers. *SID Symp. Dig. Tech. Pap.* **48**, 1960–1962 (2017).

Figures

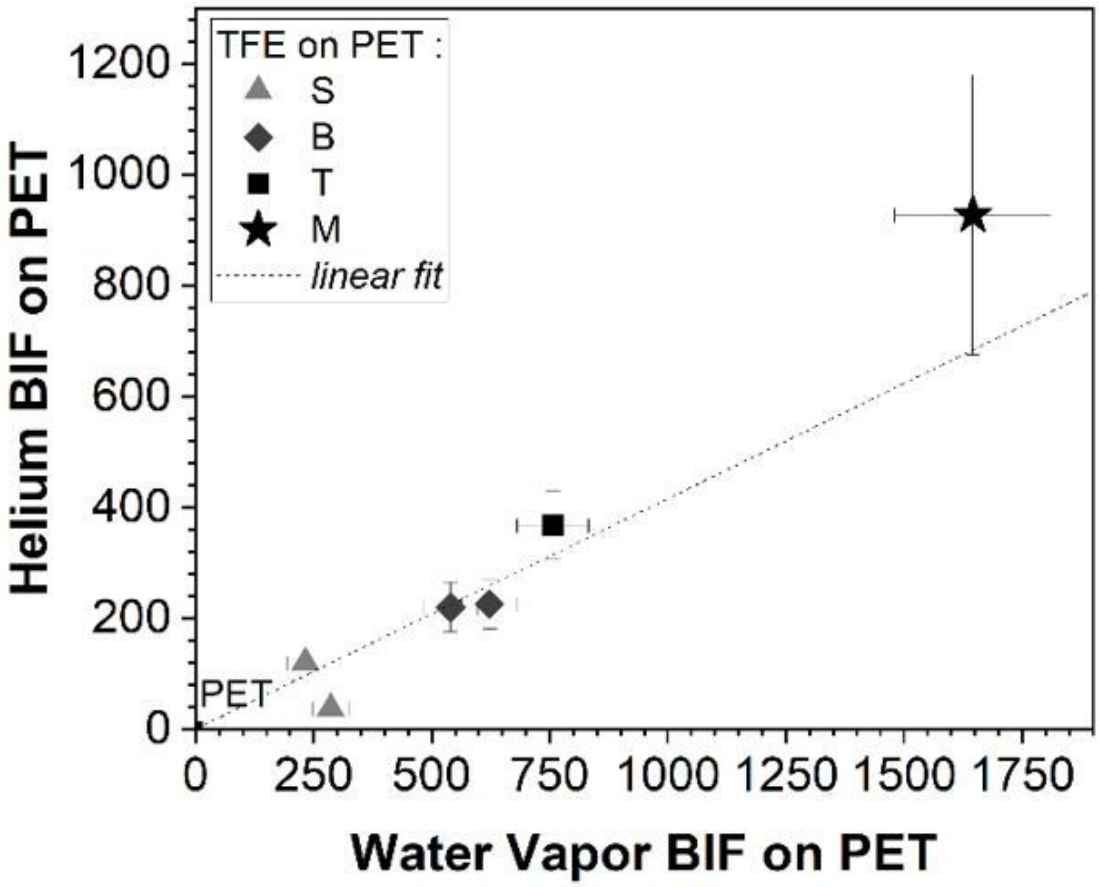

Figure 1

Linear correlation between helium BIF and Water Vapor BIF on PET substrates.

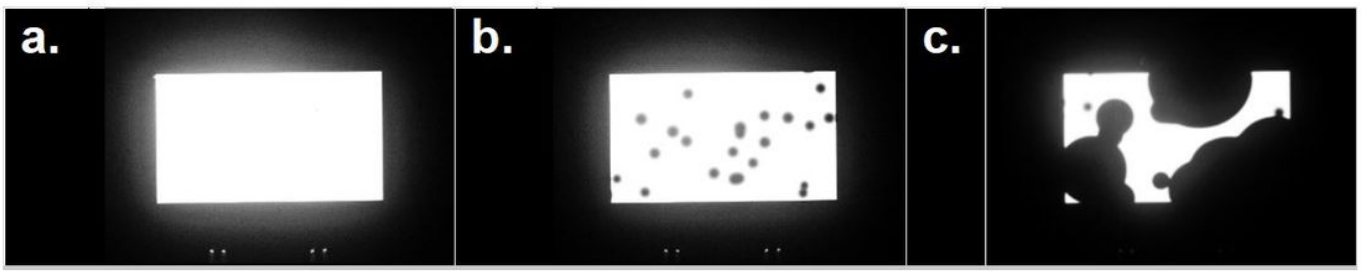

Figure 2

Defect classification on (0.38”) white top-emitting OLED devices during the weathering test (90%HR, 60 °C), (a) undamaged OLED, (b) pinhole apparition, (c) defect growth and global failure.

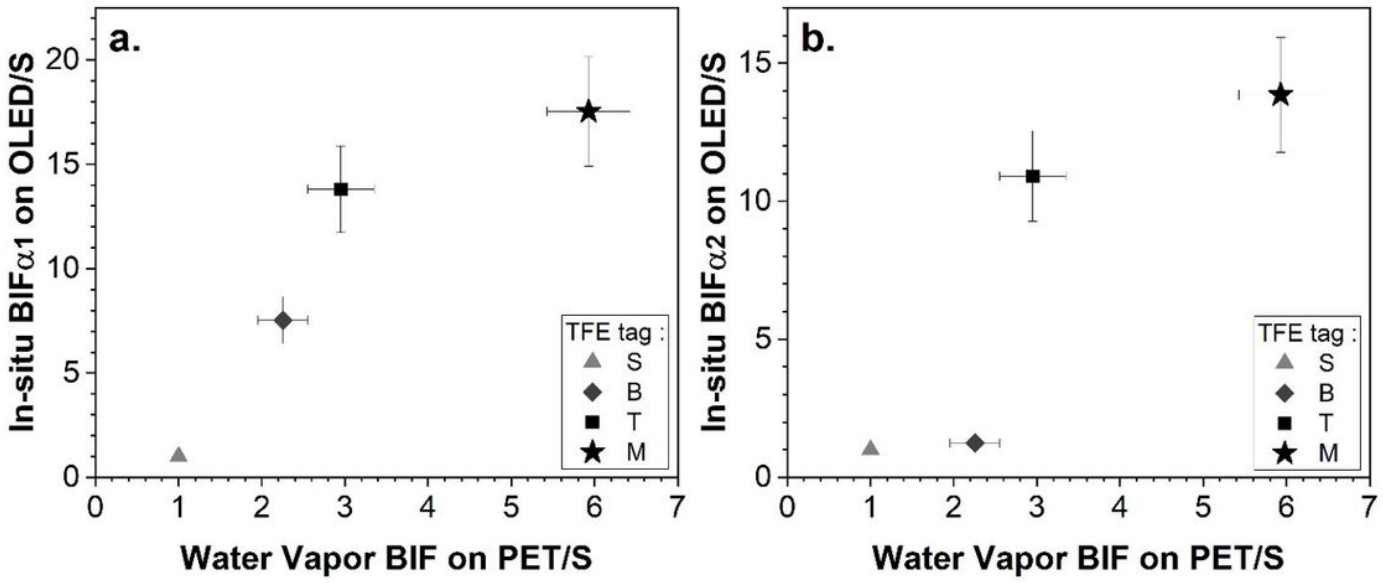

Figure 3

Correlation between in-situ OLED weathering BIF and Water Vapor BIF respectively on OLED/S and PET/S substrates. (a) short-term α1 and (b) long term α2 defect occurrence rates.

Supplementary Files

This is a list of supplementary files associated with this preprint. Click to download.

- SupplementaryInformation.pdf